

www.acsami.org Research Article

Polydimethylsiloxane-Assisted Catalytic Printing for Highly Conductive, Adhesive, and Precise Metal Patterns Enabled on Paper and Textiles

Ruisheng Guo, Haodong Li, Haoran Wang, Xiangyuan Zhao, Hong Yu,* and Qian Ye*



Cite This: ACS Appl. Mater. Interfaces 2021, 13, 56597-56606



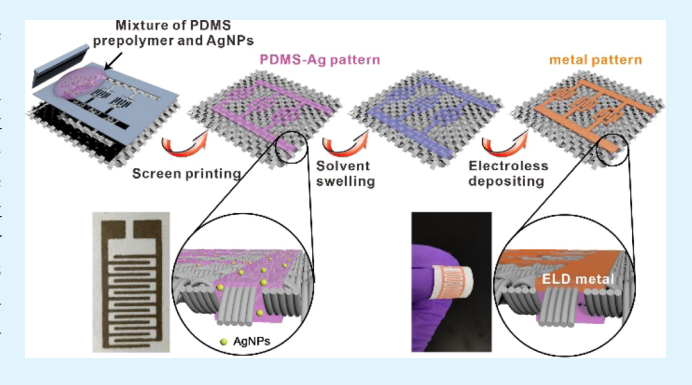
ACCESS

III Metrics & More



S Supporting Information

ABSTRACT: Paper and textile are two ideal carriers in wearable and printed electronics because of their flexibility and low price. However, the porous and fibrous structures restrain their use in printed electronics because the capillary effect results in ink diffusion. Especially, conventional metal ink needs to be post-treated at high temperatures (>150 °C), which is not compatible with paper and textile. To address problems involved in ink diffusion and avoid high-temperature treatment, herein, a new strategy is proposed: screen-printing of high-viscosity catalytic inks combined with electroless deposition of metal layers on paper and textile substrates. The ink consists of Ag nanoparticles, a polydimethylsiloxane (PDMS) prepolymer, and a curing agent. PDMS as a viscoelastic matrix of catalysts plays key roles in



limiting ink diffusion, enhancing interfacial adhesion between the substrate and metal layer, keeping metal flexible. As a demonstration, metal Cu and Ni are printed, respectively. The printed precision (diffusion < 1% on filter paper) can be controlled by adjusting the Ag content in the PDMS matrix; interfacial adhesion can be enhanced by ink coating on substrate microfibers and metal embedding into the PDMS matrix. In addition, Cu on paper shows extremely low sheet resistance (0.29 m Ω / \Box), and Cu on nylon shows outstanding foldability with a resistance of less than five times of initial resistance during 5000 folding cycles.

KEYWORDS: printed and flexible electronics, flexible metal conductors, electroless deposition, screen printing, paper electronics

■ INTRODUCTION

Conventional brittle silicon-based electronics, mainly manufactured by complicated photolithography and vacuum deposition methods with high cost, 1-3 are not compatible with the uprising flexible and wearable devices. In the past decade, tremendous interest in printed electronics, where circuits or devices can be printed on flexible and wearable substrates, have become evident. Printing methods with great patterning capability including contact (screen-printing) and noncontact [inkjet printing, three-dimensional (3D) printing] modes have been developed. These methods are compatible with solution-based and roll-to-roll processes on flexible substrates such as bendable plastics or paper 13,14 and even textiles, 15,16 thus providing feasible and effective manufacturing techniques for low cost and mass production.

Paper and textile are two ideal flexible and light-weight carriers and by far the cheapest and most exploited substrates because of environmental friendliness and recyclability of paper and the conformable and breathable properties of textiles. ^{17,18} In the meantime, their numerous microfibers are rough and rich in surface functional groups, interconnecting to form microporous platforms. These features are beneficial for binding conductive or active materials of electronic devices.

Based on the abovementioned advantages, paper- and textile-based printed circuit boards (PCBs), ¹³ radio frequency identification tags, ^{19,20} sensors, ^{21–24} energy storage devices, ^{17,25–28} and so forth ²⁹ have been deeply researched. Our previous work has also suggested that cellulose microfibers in paper-based electrodes could also act as a strong anchoring unit for upper material layers. ³⁰

As a necessary component in printed electronics, flexible and conductive material needs to be conformally applied to flexible substrates for forming an electronic circuit or electrode prior to the later-on processing. Compared with carbon materials (carbon nanotubes and graphene) and conducting polymers (polypyrrole, polyaniline, and polythiophen), metal structures are usually used owing to their excellent conductivity, chemical stability, and low price.³¹ When the metal is thin enough, it can

Received: September 21, 2021 Accepted: November 4, 2021 Published: November 16, 2021





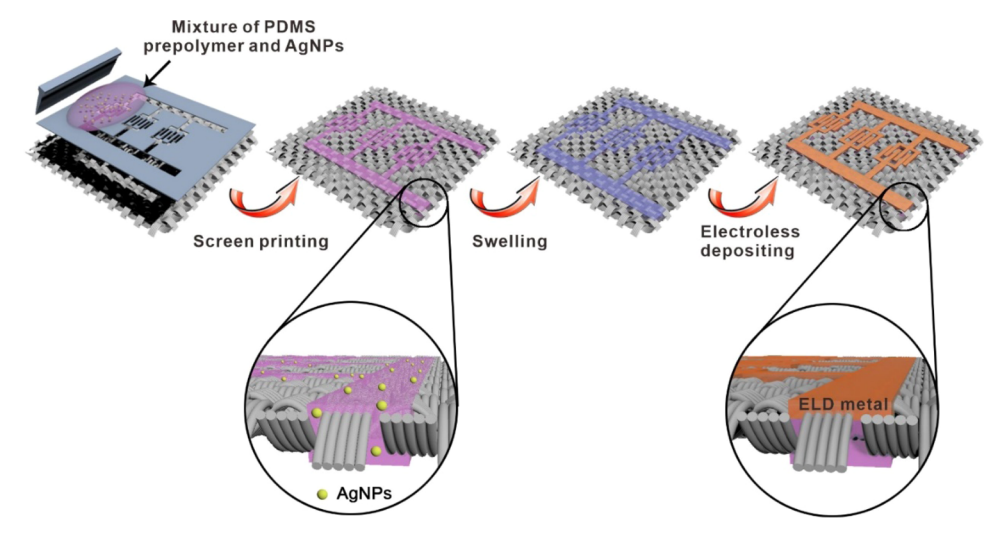


Figure 1. Schematic illustration of screen-printing metal patterns on flexible and fibrous substrates by PDMS-assisted catalytic printing.

be bent, stretched, and compressed by fitted structurization. 31-34 They have been used as interconnectors, electrodes, and contact pads for PCBs, sensors, energy generators, energystorage devices, and other electronic devices on different substrates, such as polyethylene terephthalate (PET), polyimide (PI), polyethylene naphthalene dicarboxylate, polydimethylsiloxane (PDMS), paper, textiles, and so on. 5,35-38 Applying printing technology to deposit conductive nanomaterials requires suitable formulation of ink, which is greatly related to the printing technology and wetting properties of the substrate. For paper with rough and fibrous structures, the main printing technology for metal conductors is inkjet printing, which requires diluted ink in water or organic solvents with low viscosity (0.01-0.02 Pa s).7,39,40 However, the ranges of viscosity, particle size, and low curing temperature of inks required for flexible substrates are not able to provide satisfactory electrical percolation networks on porous and rough substrates. 41 Additionally, inks easily diffuse through rough and porous substrates because of the capillary effect, especially in textile substrates. Some resolutions have been proposed to address the abovementioned problems of inks, such as using hydrophobic organosilanes to lower the surface roughness and precoating of smooth underlayers, 16,42,43 which showed unsatisfying improvement. As an alternative selection for printing metals on rough and porous textile substrates, screen-printing, capable of facilely depositing highly viscous ink, has been recently regarded as a favorable fabrication process.³⁷ When viscous conductive inks or pastes are used, the printed patterns exhibit higher conductivity than inkjet-printed metals. However, the preparation of conductive and viscous inks for screen-printing remains a challenge because a sintering process after printing is obliged. Because metal nanomaterials are surrounded by insulating organic layers from the stabilizing agents and other ink components, the electrical contacts in between are prohibited. Thus, the metal nanomaterials form a continuous phase during the sintering process with numerous interconnecting percolation paths within the printed patterns. Heat treatment is the most adopted approach for sintering. However, as the heat-sensitive nature of temperatures higher than 150 °C, sintering is not applicable for some paper and textiles, and the residues after post-treatment affect metal conductivity. Therefore, nondestructive methods are required. 35,37

Herein, we propose a simple strategy to screen-print highly conductive metal patterns with two aspects of advantages. On the one hand, the PDMS liquid mixture consisting of a prepolymer and curing agent is selected as a thickener and binder because of its relatively high viscosity of ca. 5500 mPa s and low surface tension of ca. 21 mN m⁻¹.⁴⁴ It is suitable for screen-printing by adding some additive agents.⁶ The cured PDMS processes the well-known flexibility, stretchability, and biocompatibility at the same time, which is usually used in flexible and wearable electronics. On the other hand, Ag nanoparticles (AgNPs), better for screen-printing ink with less aggregation and blocking than nanowires, 45-49 are embedded into the PDMS matrix acting as catalytic seeds to grow thick metal layers on the surface of PDMS by electroless deposition (ELD). The postdeposition of metal forms a complete metal layer above the nonconductive PDMS and could improve the conductivity of the metal pattern. Because the ink rheology can be controlled by adjusting the AgNP content, high-precision patterns can be achieved; metal conductivity also can be controlled by adjusting the ELD time but not the ink thickness, therefore high conductivity can be completed. More important is that PDMS acts as an adhesive agent in addition to playing the role of a matrix and thickener, greatly enhancing the adhesion between metals and paper/textile microfibers. As far as we know, although printing Ag specimens as catalytic seeds for sequential ELD metal and PDMS as a matrix carrier of conductive Ag patterns have been reported in a few studies, 19,50-53 the strategy of using PDMS as a matrix carrier of catalysts has not been reported. PDMS as an elastic and adhesive interfacial layer between the rough substrate and metal can ensure excellent flexibility of paper- and textile-based metal.

EXPERIMENTAL SECTION

Materials. The PDMS prepolymer and the curing agent (Sylgard 184) were purchased from Dow Corning. AgNPs (99.5% metals basis, 60–120 nm, containing colophony dispersant) were purchased from Aladdin Co. Ltd. 3-Aminopropyltriethoxysilane (APTES) was purchased from J&K Chemicals, and all other chemicals were purchased from Sigma-Aldrich. Filter paper, nylon fabrics, and kimwipes were commercial products.

Ink Preparation. AgNPs capped with colophony were modified with APTES by immersing AgNPs into APTES ethanol solution (containing 5 vol % H₂O), the mass of APTES was 5 wt % of the total

mass of AgNPs and APTES. After mixing and stirring for 12 h, vacuum filtration was performed, and the obtained product was dried in a vacuum drying oven at 80 °C for 12 h and dispersed for use. The ink (denoted as PDMS-Ag) was prepared by mixing the PDMS prepolymer, curing agent, and AgNPs. The mass ratio of PDMS prepolymer to curing agent was fixed at 1: 0.1. The mass percentage of AgNPs in composite ink was varied from 31.25, 40.54, 47.62, 53.19 to 57.69% (the mass ratio of AgNPs to PDMS prepolymer was varied from 0.50, 0.75, 1.00, 1.25 to 1.50).

Fabrication of Metal Patterns. As shown in Figure 1, first, ink patterns were screen-printed onto the surfaces of flexible substrates such as filter paper, nylon fabrics, and kimwipes, and then cured at 80 °C for 2 h in an oven; second, ink patterns on substrates were immersed into acetone or tetrahydrofuran (THF) for 30 min to swell PDMS-based ink because small solvent molecules could diffuse into large cross-linked networks and swell PDMS;^{54,55} third, substrates with swelled inks were immersed into ELD solution for in situ depositing metal layers on ink patterns, the ELD time was varied from 30, 60, 120, 180 to 240 min. The ELD Cu solution was prepared at room temperature by dissolving HCHO (15 mL L⁻¹), CuSO₄ (15 g L⁻¹), C₄H₁₂KNaO₁₀ (14 g L⁻¹), 2,2'-bipyridyl (0.02 g L⁻¹), C₁₀H₁₄N₂Na₂O₈ (19.5 g L⁻¹), NaOH (14.5 g L⁻¹), and K₄Fe(CN)₆ (0.01 g L⁻¹) in deionized water.³⁶ The ELD Ni was prepared in a plating bath by mixing 1 g L⁻¹ dimethylamine borane (DMAB) and nickel stock solution (40 g L⁻¹ Ni₂SO₄·5H₂O, 20 g L⁻¹ sodium citrate, and 10 g L^{-1} lactic acid) with a ratio of 1:4 (v/v) and adjusting the pH \approx 8 with ammonia. A nickel stock solution was prepared in advance, and the DMAB aqueous solution was prepared separately. All ELD experiments were carried out at room temperature.

Materials Characterization. The rheological properties of the composite inks were measured at 25 °C using a rotational rheometer (HAAKE MARS III, Thermo fisher Ltd., Germany) fitted with a parallel plate geometry. Its apparent viscosity was measured as a function of shear rate using a rotational stress sweep from 0.01 to 100 s⁻¹. The Fourier transform infrared spectroscopy (FT-IR) spectra of samples in the range of 4000-500 cm⁻¹ were recorded using an IS-10 infrared spectrometer to analyze the functional groups. The morphologies of PDMS-Ag ink, Cu/PDMS-Ag, and Ni/PDMS-Ag on filter paper and the corresponding energy-dispersive X-ray spectroscopy (EDS) spectra were observed by field-emission scanning electron microscopy (FESEM) (Zeiss Gemini-500) at an acceleration voltage of 5 kV. An optical microscope was also used to observe the surface morphologies of substrates and PDMS-Ag inks and metal patterns on different substrates. The roughness of the samples was measured using a surface roughness tester (model 2300A-R) from the HMCT GROUP. A Bruker D8 X-ray diffractometer recorded X-ray diffraction (XRD) profiles from 5 to 80° of the as-prepared samples with Cu K α radiation (λ = 0.154 nm). The X-ray photoelectron spectroscopy (XPS) spectra were collected using an Axis Supra X-ray photoelectron spectrometer with a monochromated Al Ka X-ray source. The surface tension of the PDMS-Ag ink was determined using the ring tension method using a surface interfacial tension measuring instrument (JK99F, Zhongchen, China).

Electrical and Mechanical Characterization. Bending and folding tests of Cu/PDMS-Ag on different substrates were conducted using a home-built and motorized uniaxial stretcher. The resistances were measured using the two-point probe method with a Keithley 2400 sourcemeter and collected using a computer-controlled software. Sheet resistances were measured using the four-point probe method with HP 504 (Guangzhou 4 Probes Tech.). A reciprocating friction test was conducted against a steel ball pair by loading 0.5 N using a multifunctional friction tester (Lanzhou Huahui Instrument Tech. Co., Ltd.). The adhesion of the copper pattern was estimated using a set of tools (QFH-HG600, Huaguo Precise Instrument Corp., China).

RESULTS AND DISCUSSION

Fabrication of Metal Patterns by PDMS-Assisted Catalytic Printing. Before fabricating metal patterns, the ink was first prepared by mixing AgNPs and the PDMS prepolymer with a curing agent. The purchased AgNPs were capped using a colophony dispersant to prevent AgNPs from aggregating, which, however, cannot form uniform dispersion with the PDMS prepolymer and curing agent, resulting in large aggregation when being printed on the flat PET surface, as shown in Figure S1a and on the paper substrate, as shown in Figure S1b. To improve the dispersion of AgNPs in the PDMS matrix, APTES was used to modify the colophony-ended AgNPs. The FT-IR spectra of AgNPs before and after modification using APTES are shown in Figure S2. After modification, three new peaks were detected in the spectrum as compared with colophony-capped AgNPs, corresponding to the groups of Si-C stretching vibrations, -NH bending vibrations, and -NH2 stretching vibrations broad at 807, 1543, and 3452 cm⁻¹, respectively, suggesting that APTES was assembled onto AgNP surfaces. After modification, uniform dispersion of AgNPs in PDMS was obtained. Figure S1c,d shows that uniform PDMS-Ag inks were printed on PET and paper substrates, respectively.

Figure 1 shows the schematic illustration of screen-printing inks and forming metal (Cu or Ni) patterns on paper or textile substrates. The patterned metal conductors can be facilely achieved using one printing process and subsequent two successive solution-immersion steps, that is, printing PDMS-Ag catalytic ink, solution-processing using a water-soluble solvent (acetone or THF), and solution-processing using ELD aqueous solution. During the printing process, PDMS-Ag composite inks would spread slightly on the substrate microfibers and coat them because of the low surface tension values of PDMS (21 mN m⁻¹) and PDMS-Ag ink (45.3 mN m⁻¹), which are less than the surface energies of nylon and cellulose paper (> 45.3 mJ m⁻²).⁵⁶ After being printed and solidified at 80 °C, PDMS-Ag inks on porous substrates were immersed into solvents to swell PDMS and expose the AgNPs. Also, the swelled inks on substrates were immediately immersed into ELD aqueous solutions to grow metal nanoparticles on the active sites of the exposed AgNPs. It is noted that organic solvent treatment is an essential step. The control experiment without organic solvent treatment displayed that ELD metal cannot be deposited. In addition, it is found that THF with a high swelling coefficient could promote metal growth more easily compared with acetone; this phenomenon will be analyzed in another section below.

Proper PDMS-Ag ink should meet two requirements for the screen printing and formation of Cu patterns on the substrate surface. On the one hand, feasible rheological properties of the ink are required for screen-printing technology. On the other hand, AgNPs dispersed in the PDMS matrix need to be properly adjusted to catalyze the growth of a consecutive ELD metal layer. As the Ag content in the PDMS-Ag ink greatly affects the rheological properties and catalytic performance of the ink, the mass ratio of AgNPs to PDMS was investigated. In general, the ink should possess high viscosity to stabilize on the printing board at a low shear rate, however, change to a very low viscosity during printing at a high shear rate and finally is capable of returning to its high viscosity after printing.⁵⁷ The ink consisted of the PDMS prepolymer, curing agent, and AgNPs. The mass ratio of PDMS prepolymer to curing agent was fixed at 1:0.1, and that of AgNPs to PDMS prepolymer varied from 0 (denoted as ink₀), 0.50 (denoted as ink_{0.50}), 0.75 (denoted as $ink_{0.75}$), 1.00 (denoted as $ink_{1.00}$), 1.25 (denoted as $ink_{1.25}$) to 1.50 (denoted as $ink_{1.50}$). The viscosity properties of ink₀, ink_{1.00}, ink_{1.25}, and ink_{1.50} with shear rates between 10^{-3}

and 10^2 s⁻¹ were characterized (Figure 2a). The apparent viscosities of ink₀, ink_{1.00}, ink_{1.25}, and ink_{1.50} at a shear rate of

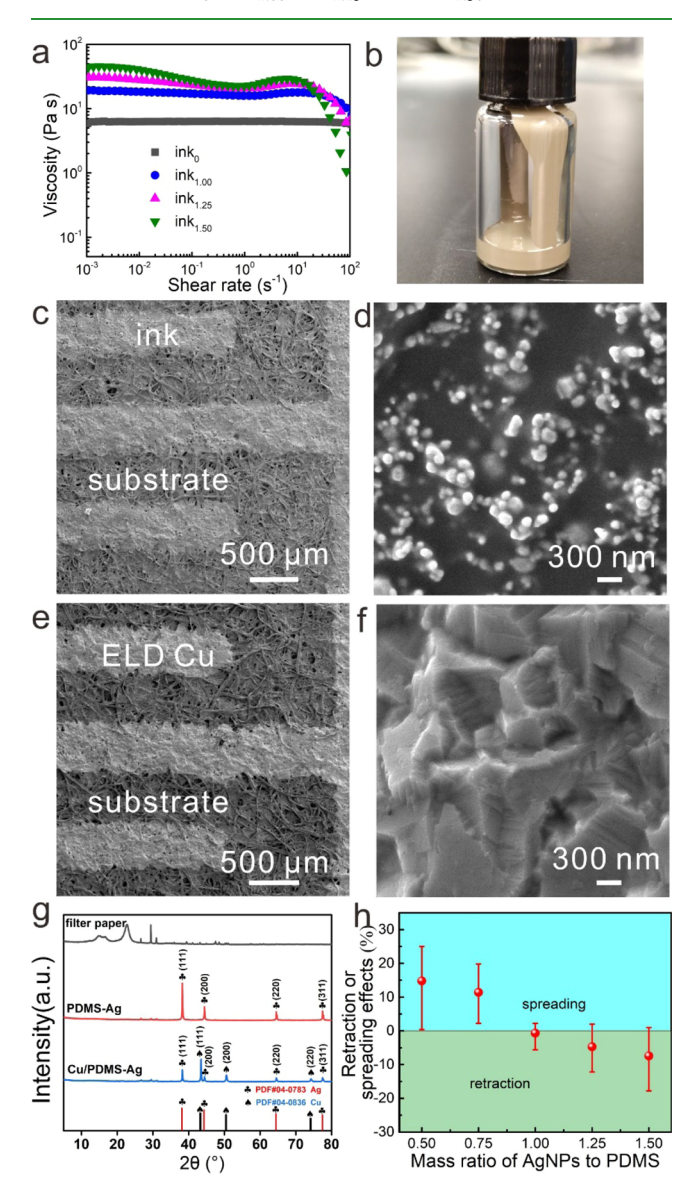


Figure 2. (a) Rheological properties of inks with different Ag mass fractions. (b) Digital photograph of PDMS-Ag $\operatorname{ink}_{1.00}$ in a bottle. (c) Low- and (d) high-magnified SEM images of PDMS-Ag $\operatorname{ink}_{1.00}$ with an interdigital pattern printed on the filter paper surface. (e) Low- and (f) high-magnified SEM images of the ELD Cu layer grown on patterned ink. (g) XRD spectra of filter paper, PDMS-Ag on filter paper, and Cu/PDMS-Ag on filter paper. (h) Spreading or the retraction effect of inks with different Ag mass fractions printed on filter paper along surfaces.

 $0.001~{\rm s}^{-1}$ were 5894, 19,308, 30,481, and 44,265 mPa s, respectively. The viscosity increased with the increasing fraction of AgNPs. All tested samples displayed a shearthinning effect overall under the shearing window. In addition to the ink₀ sample, all other samples exhibited shear-thickening behavior from 1 to 6 s⁻¹ in a narrow range, which might be attributed to the aggregation of AgNPs during shearing. After that, viscosity dramatically decreased with a continuously increasing shear rate, which may be derived from the disruption of the noncovalently linked network in colloidal gels by high shear. ⁵⁸ This behavior enables the continuous

extrusion of ink through the screen mesh under moderate conditions. Thereby, $ink_{1.00}$, $ink_{1.25}$, and $ink_{1.50}$ are suitable for screen-printing technology. An excessive amount of silver (mass ratio of AgNPs to PDMS > 1.50) increased the viscosity significantly, thus making printing difficult, while less amount of AgNPs (mass ratio < 1.00) was unable to grow continuous ELD metal layer. Figure 2b shows the digital photograph of ink_{1,00}, which was used to print an interdigital pattern on filter paper by screen-printing technology. The mask of the screen pattern contained 16 fingers, and both the finger width and the gap between the neighboring fingers were 500 μ m. After printing the ink, the as-printed finger width and finger gap maintained the equal value of \sim 500 μ m observed from the low-magnification scanning electron microscopy (SEM) image (Figure 2c) and digital image (Figure S3a). The surface was rough and rugged because of the roughness of filter paper. The high-magnification SEM image in Figure 2d exhibits the surface morphology of the printed ink on filter paper. Small white dots with nanoscale dispersed in PDMS-Ag ink, and the sizes were more than 120 nm (purchased size <120 nm). EDS mapping displays that Si and Ag elements are located in the same area, as shown in Figure S4. It can be deduced that AgNPs were encapsulated by PDMS. After Cu deposition on the ink pattern by ELD, the obtained finger width and finger gap values were the same (\sim 500 μ m) as those of the ink pattern (Figures 2e and S3b). The Cu layer was deposited on the surface and covered PDMS-Ag, forming a relatively compact Cu film, as shown in Figure 2f. This indicates that Cu particles gradually bridged the gaps between AgNPs as catalytical Cu growth. Because the gaps between AgNPs were not more than 2 μ m, as shown in Figure 2d, the diffusion of the finger width after Cu deposition was not more than 1%, duplicating the ink pattern profile. The XRD data (Figure 2g) show a Cu/PDMS-Ag diffraction pattern with crystalline peaks on the surface of filter paper. The peaks positioning at 43.45, 50.60, and 74.2° perfectly matched the (111), (200), and (220) planes of the Cu layer, respectively. The peaks locating at 38.2, 44.4, 64.6, and 77.5° corresponded to (111), (200), (220), and (311) planes of AgNPs. Other peaks with lower intensity of Cu/PDMS-Ag were attributed to the filter paper. In addition, we also investigated the printing capability of the rest inks (ink_{0.50}, ink_{0.75}, ink_{1.25}, and ink_{1.50},) on rough filter paper. As ink_{0.50} and ink_{0.75} had less amount of AgNPs, they diffused on filter surfaces because of their lower viscosity, and the resulting Cu layers were discontinuous after the ELD process; while ink_{1,25} and ink_{1,50} obviously retracted because of their higher viscosity. The spreading and retraction percentages are shown in detail in Figure 2h, and their optical images are shown in Figure S5. Thus, for the filter paper, the best ink used to print a highly precise pattern is the ink_{1.00}. Importantly, the long shelf life of ink_{1.00} up to 5 months demonstrates its excellent stability. Clear and almost identical ink_{1.00} patterns printed using liquid ink stored for different months and the Cu pattern on filter paper can be seen in Figure S6a, and there was a similar electrical stability trend during 100 bending cycles between Cu lines printed using fresh ink and old ink stored for 5 months (Figure S6b). Thus, in the following experiments, the "ink" is referred to $ink_{1.00}$, if not specified otherwise. In a word, a high-precise metal pattern can be facilely achieved by the above-demonstrated PDMS-assisted catalytic printing, which consists of one printing and two successive solutionimmersion steps at a low temperature (the cured temperature of PDMS-Ag ink is ≤ 80 °C).

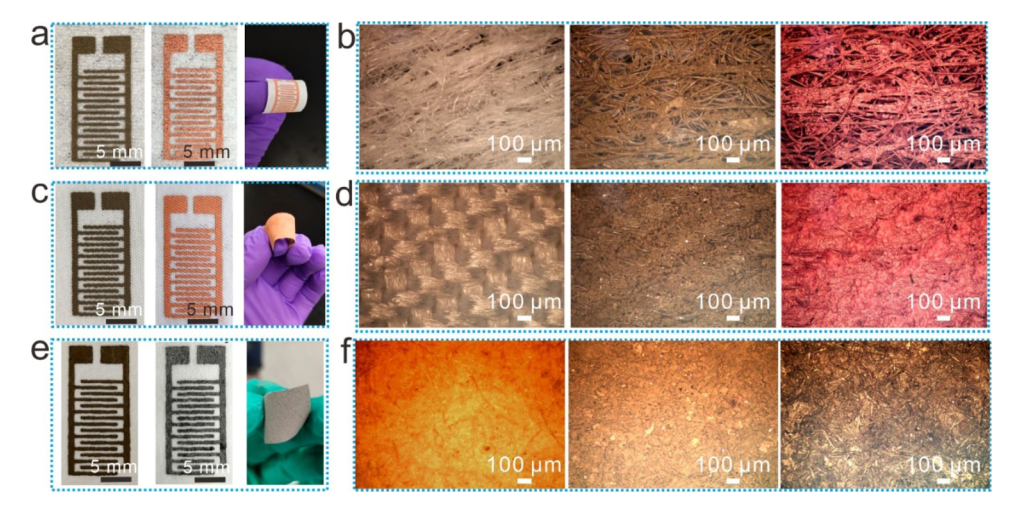


Figure 3. (a) Photographs of PDMS-Ag ink, Cu/PDMS-Ag, and flexible Cu/PDMS-Ag on kimwipes and (b) optical images of bare kimwipes, PDMS-Ag ink on kimwipes, and Cu/PDMS-Ag on kimwipes. (c) Photographs of PDMS-Ag ink, Cu/PDMS-Ag, flexible Cu/PDMS-Ag on nylon fabric and (d) optical images of bare nylon fabric, PDMS-Ag ink on nylon, and Cu/PDMS-Ag on nylon. (e) Photographs of PDMS-Ag ink, Ni/PDMS-Ag, and flexible Ni/PDMS-Ag on filter paper and (f) optical images of bare filter paper, PDMS-Ag ink on filter paper, and Ni/PDMS-Ag on filter paper.

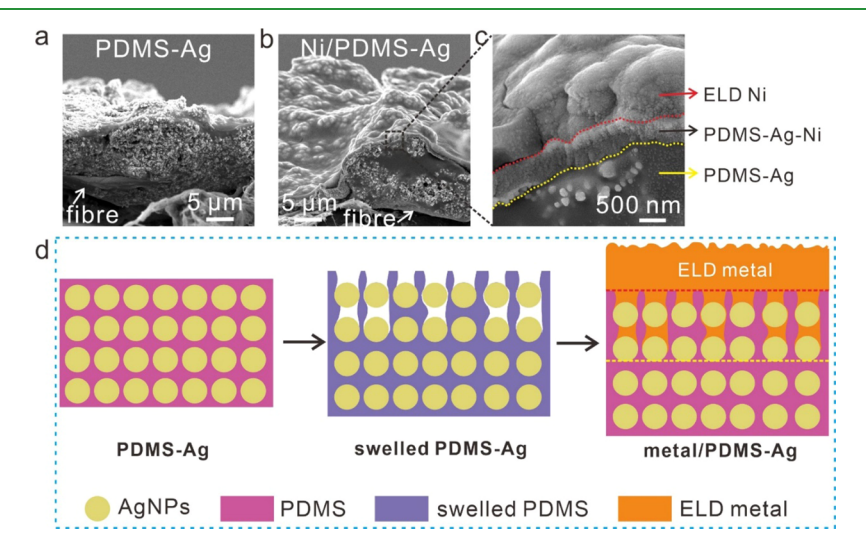


Figure 4. (a) Cross-section SEM image of PDMS-Ag ink printed on filter paper. (b) Cross-sectional SEM image of Ni/PDMS-Ag on filter paper and (c) corresponding magnification view. (d) Schematic illustration of ELD metal growing from the swelled PDMS-Ag composite.

Versatility of PDMS-Assisted Catalytic Printing. PDMS-assisted catalytic printing is versatile for most of the rough substrates with porous structures consisting of microfibers. Figure 3 shows the inks and metal patterns printed on different types of substrates, including ink and Cu patterns on kimwipes (Figure 3a), ink and Cu patterns on nylon fabric (Figure 3c), and ink and Ni patterns on filter paper (Figure 3e). Figure 3a,c display a slight diffusion of Cu on kimwipes and nylon because of their rougher and more porous surfaces than filter paper, as verified by the optical images of bare substrates in Figure 3b,d. After printing ink and depositing metal, clear microfiber structures can be seen for kimwipes, whereas microfibers were mostly covered by ink, and the rough surface was filled up by Cu for nylon. In addition to Cu, metal Ni can also be deposited using this PDMS-assisted catalytic printing method (Figure 3e,f). The peaks from 850 to 880 eV indicate the presence of metallic Ni in Ni/PDMS-Ag on filter paper in the XPS spectra shown in Figure S7.59 All the metal patterns on flexible substrates showed conformal flexibility, as shown in Figure 3a,c,e. In addition, we carried out control

experiments on flat substrates such as PET and PI. It was found that the ink film of PDMS-Ag would peel off from flat substrates during the swelling process via solvents, suggesting that PDMS-Ag can wrap up microfibers of fibrous substrates after ink printing. At the same time, no stripping from porous substrates verified very strong adhesion between PDMS-Ag composites and fibrous substrates. In summary, different metals can be printed on various flexible substrates with fibrous structures by PDMS-assisted catalytic printing.

Strong Adhesion between the Metal Pattern and Substrate. Furthermore, the growth mechanism of ELD metal from PDMS-Ag ink was studied. The cross-section morphologies of PDMS-Ag ink and Ni/PDMS-Ag on filter paper were observed to clarify the interfacial relationship of the substrate/PDMS-Ag and PDMS-Ag/ELD metal. The cross-section view and EDS mapping of PDMS-Ag ink (Figures 4a and S8a, respectively) show that PDMS-Ag is conformally coated on microfibers with a thickness of $\sim 10~\mu m$, which further confirms the interface adhesion between PDMS-Ag and the substrate discussed in the previous paragraph. After the deposition of Ni,

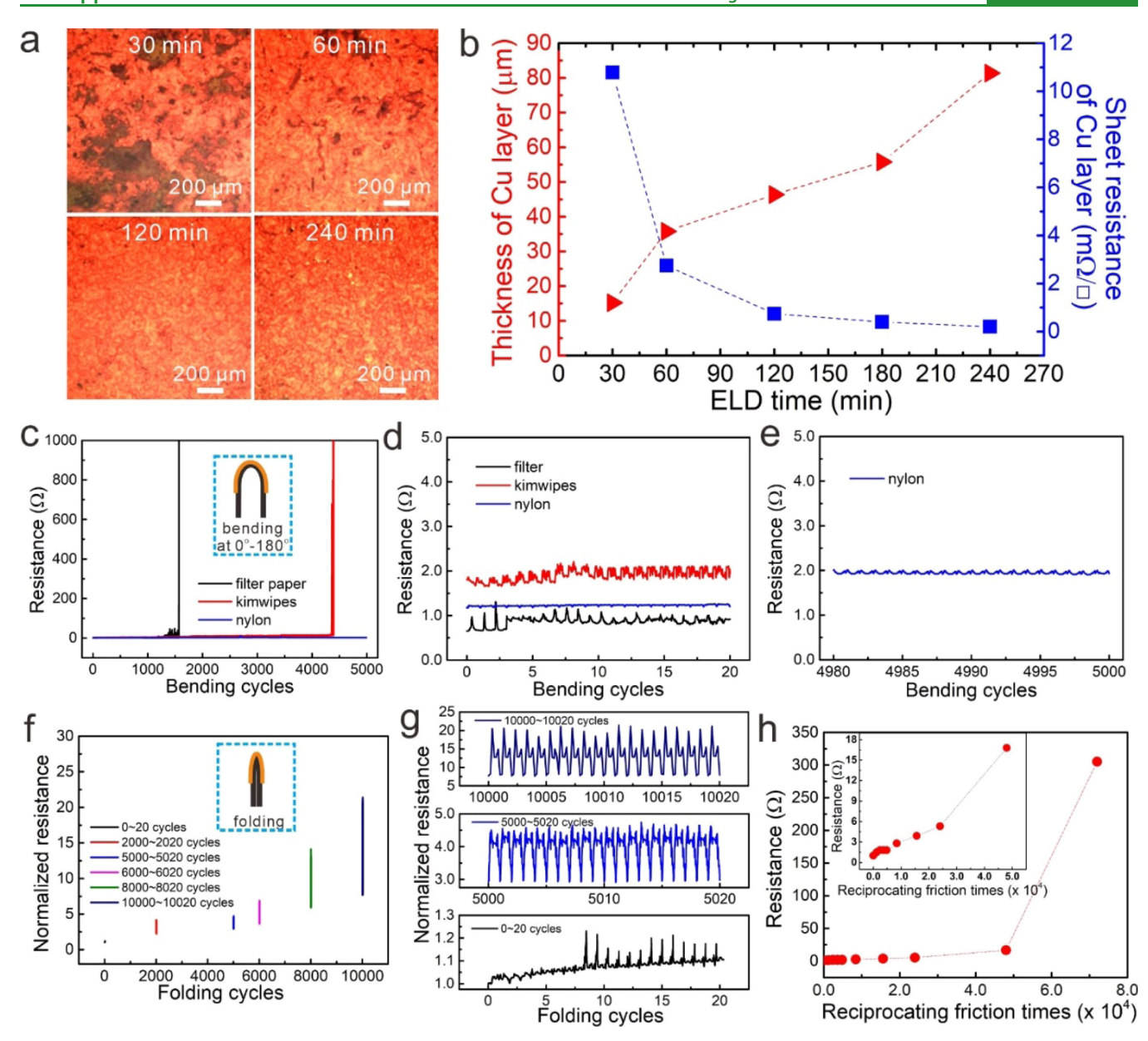


Figure 5. (a) Optical images of Cu layers deposited on filter paper with different ELD times, ranging from 30, 60, 120 to 240 min. (b) Thickness and sheet resistance of Cu layers with ELD deposition time. (c) Resistance changes of Cu/PDMS-Ag on different substrates (filter paper, kimwipes, and nylon) with an increase in bending cycles. (d) and (e) Detailed plots of Figure 5c during 0–20 bending cycles and 4980–5000 bending cycles; inset shows the maximum bending state of the sample. (f) Normalized resistances of the Cu layer on nylon as a function of folding cycles. (g) Detailed plots of Figure 5f in different windows including 0–20 folding cycles, 5000–5020 folding cycles, and 10,000–10,020 folding cycles; inset shows the maximum folding state of the sample. (h) Resistance change with reciprocating friction times under 0.5 N loading; inset shows the magnified plot.

a ductile and continuous Ni layer was observed covering the top of the PDMS-Ag surface, as confirmed by the cross-section image and EDS mapping of Ni/PDMS-Ag in Figures 4b and S8b, respectively. From the magnified image in Figure 4c of the marked area of Figure 4b, three distinctly different layered morphologies were clearly detected at the interface between PDMS-Ag and ELD Ni: (1) the PDMS-Ag composite layer below the yellow dot line (yellow arrow); (2) the ELD Ni layer above the yellow dot line (red arrow); (3) the intermediate layer between the red and yellow dot lines (black arrow), whose relatively rough texture is in between the ELD Ni layer and PDMS-Ag layer; thus, it is deduced to be the PDMS-Ag-Ni composite. The possible formation process of the composite is illustrated in Figure 4d. The printed PDMS-Ag layer on the

substrate cannot directly catalyze the growth of ELD metal because AgNPs were encapsulated by PDMS without exposed active sites. Therefore, solvent swelling for the PDMS-Ag layer was necessarily conducted to open PDMS and expose AgNPs being accessible by the solvent. The swelled PDMS-Ag layer on the substrate was immediately put into ELD solution to grow metal. The fast immersion aims at preventing the solvent from volatilizing in the atmospheric environment. Solvents (acetone or THF) used are water-soluble to mix with ELD aqueous solution easily, and then, ELD solution can approach AgNPs for the nucleation of ELD metal. It is worth noting that THF-swelled PDMS-Ag catalyzed the growth of ELD metal more easily, and the as-prepared metal layer had better continuity than that swelled by acetone because of a larger swelling ratio

of THF for PDMS. The data in the literature show a swelling ratio of 1.38 for THF but only 1.06 for acetone.⁵⁴ A larger volume of the swelled PDMS-Ag implies more exposed AgNPs, which is also beneficial for shortening the ELD deposition time and thickening the interface layer of the PDMS-Ag-ELD metal. The thick PDMS-Ag-Ni composite layer of ~500 nm shown in Figure 4c enhanced the adhesion between the PDMS-Ag composite and the ELD metal in this work. There was almost no gap between the metal layer and the interface layer (also can be seen in Figure S9 without sign). At the same time, PDMS-Ag coated microfibers improved the adhesion between the cured PDMS-Ag composite and substrates with porous and microfibers. Thereby, metal patterns can firmly stick to paper and textiles. To demonstrate the strong adhesion, an adhesion cross-cut test was conducted for the Cu layer on filter paper. As presented in Figure S10a, the Cu layer had not been destroyed, and the scotch tape had no adhered Cu particles. Furthermore, a strong adhesive cellophane tape was used to tear the Cu layer, not only no peeling off of the Cu layer had been observed but also the glue on the tape was torn by the Cu layer, as shown in Figure S10b.

Electrical and Mechanical Properties of Metal Patterns on Flexible Substrates. Printed flexible metal patterns on different substrates are mainly used in flexible and wearable electronics, so their electrical and mechanical properties were investigated. The resistance of Cu/PDMS-Ag fabricated by screen-printing ink on filter paper in whole was investigated by adjusting the ELD time and fixing other parameters. Figure 5a presents the optical images of samples after depositing the Cu layer for 30, 60, 120, and 240 min. Only a partial region of the ink area was covered by Cu for an ELD time of 30 min; then, the Cu area enlarged as the ELD time increased to 120 and 240 min. The mean thicknesses (shown on the left in Figure 5b) of the Cu layer were 15.2, 35.8, 46.4, 55.8, and 81.4 μ m corresponding to the ELD time of 30, 60, 120, 180, and 240 min. The mean thicknesses of the filter paper and PDMS-Ag ink were 185 and 6.8 μ m, respectively. All thicknesses were measured using a vernier caliper. It can be found that the thickness of ELD Cu linearly increased with the increase in ELD time roughly. Their sheet resistances measured using the four-point probe method were also plotted (right side, Figure 5b). The sample with 30 min ELD was almost nonconductive, but the sheet resistance dramatically reduced to 3.67, 0.74, 0.39, and 0.29 m Ω/\Box with increasing ELD time. For the sample with 240 min ELD, its resistivity dropped to $2.36 \times 10^{-8} \,\bar{\Omega}$ m, approaching the value of bulk Cu (1.70 \times 10⁻⁸ Ω m). These low sheet resistance and resistivity prove that as-printed flexible and wearable conductors have excellent conductivity. Compared with other PDMS-based composite conductors, although many conductive fillers (AgNPs, Ag nanowires, Cu nanowires, or Au nanowires) were used to enhance the conductivity of the flexible composite, their conductance is relatively lower owing to the existence of PDMS. 60-62 For example, Alexandre Larmagnac et al. reported that conductive tracks were fabricated by screen-printing the composite ink of PDMS and Ag nanowires, and the traces exhibited a relatively low conductivity of 18,168 S cm⁻¹ (\sim 1/35 of bulk conductance).⁴⁷ Furthermore, these printed Cu layers manifested outstanding thermal stability. Figure S11a shows the changes in the normalized resistances of Cu/filter paper during heating for 50 h when they were placed in an oven at 80 and 180 °C. There were negligible changes in resistances, and no oxide was

detected for the sample after heating at 180 °C for 50 h, as indicated by XRD in Figure S11b. To demonstrate the application in flexible and wearable electronics, the bending tests were conducted using Cu strips on flexible filter paper, kimwipes, and nylon substrates. All samples were cut into 3 cm in length and 0.5 cm in width, and the ELD Cu time was 120 min. The mean thicknesses of used samples were 238 μ m for the filter paper, 259 μ m for kimwipes, and 319 μ m for nylon. Their respective initial resistances were 0.65, 1.81, and 1.17 Ω . The different initial resistances are determined by their inherent fiber structures mentioned in the previous section. The result of the bending test (Figure 5c) presents a stable resistance below 2.5 Ω before 1000 cycles for the filter paper; however, a sudden resistance change occurred after 1560 bending cycles. The resistance of kimwipes remained stable below 15.0 Ω before 4000 cycles, and the change occurred after 4370 cycles. In comparison, the resistance of nylon remained stable until 5000 cycles. Figure 5d presents their detailed information during 0-20 bending cycles. All samples displayed fluctuations of resistances during one cycle because of different bending angles, but their resistances were no more than 1.3 Ω for filter paper and 2.2 Ω for kimwipes. The resistance of nylon showed almost no change with a starting resistance of 1.17 Ω and the highest resistance of 1.99 Ω during 5000 bending cycles and remained constant even in the last 20 cycles (Figure 5e). The difference in bendability among different samples could originate from their material and structure properties. Filter paper and kimwipes are made of plant fibers, while nylon is made of manmade fibers. The toughness of manmade fiber is superior to that of plant fiber, and the rougher structure of nylon is beneficial for releasing bending stress and thus maintaining the electrical contact during bending as compared with the other two substrates (the mean roughness of nylon and filter paper is shown in Figure S12 and Table S1). Kimwipes' structure is looser than that of filter paper, so it has room to cushion the stress from bending, resulting in better flexibility. To further demonstrate the practical application in flexible and wearable electronics, an electronic circuit was printed on polyester/cotton blend fabric, and nine light-emitting diodes (LEDs) were attached to the circuit. No brightness change of LEDs when being bent (Figure S13) suggests the good flexibility of printed metals on

Expect from bending, the folding capability is another important flexible index. The foldability test of Cu on nylon was conducted for 10,020 cycles, as shown in Figure 5f,g. The folded sample was 2 cm in length and 0.5 cm in width, and its initial resistance was about 0.49 Ω . The normalized resistance was used to help understand. We measured six segments, respectively, ranging from 0-20 cycles, 2000-2020 cycles, 5000-5020 cycles, 6000-6020 cycles, 8000-8020 cycles to 10,000-10,020 cycles; each segment had 20 folding cycles, and resistance changes were recorded. The resistance and its fluctuation were very small in the first 20 cycles; however, not only the low value at the flattened state but also the high value at the folded state, all increased with prolonged cycle times, together with the fluctuation range (Figure 5f). Figure 5g presents the detailed resistance changes during the ranges of 0-20 cycles, 5000-5020 cycles, and 10,000-10,020 cycles. The normalized resistance changed from 1.0 to 1.2 during the first 20 cycles and the increment was 0.2; that changed from 3.0 to 4.5 and the increment was 1.5 during 5000-5020 cycles, that changed from 7.1 to 20 and the increment was 12.9 during

 $10,\!000-10,\!020$ cycles. The resistance change was derived from crack formation, and cracks became more and longer with increasing folding cycles. Even so, the resistance of the sample was no more than $10~\Omega$ after 10,000 folding cycles, which suggests that the printed Cu/PDMS-Ag on nylon has outstanding foldability.

Finally, the wear-resistance ability was also tested because wearable electronics would experience wear and friction sometimes. The test result was indicated by measuring the electrical resistance (Figure 5h) at both ends of Cu on nylon with a width of 0.6 cm and a length of 1.2 cm. The reciprocating friction was conducted along the width of sample central, one-way travel was 0.6 cm, and one-cycle travel was 1.2 cm. The initial resistance was 1.0 Ω ; after friction, the resistance gradually increased to 1.5 Ω at 1200 cycles, 1.8 Ω at 4800 cycles, 2.8 Ω at 8400 cycles, 3.9 Ω at 15,600 cycles, 5.3 Ω at 24,000 cycles, and to 16.8 Ω at 48,000 and 305 Ω at 72,000 cycles. The increase trends can be divided into three parts: (1) the resistance increases 5.3 times from 0 to 24,000 cycles; (2) 3.17 times from 24,000 to 48,000 cycles; and (3) 18.15 times from 48,000 to 72,000 cycles. The reason for different change rates in different parts will be studied in the future. Furthermore, the wash resistance of the Cu layer printed on textiles was tested by soaking the textile in water under vigorous stirring at 1000 rpm for 14 h. Specifically, pure water was used for the first 10 h, and a clothing cleanser was then added and stirred for another 4 h. The change in sheet resistance with time is shown in Figure S14. The sheet resistance increased with washing time from initial 6.7 m Ω/\Box to final 14.5 m Ω/\Box , but it was still very low, suggesting that the metal layer printed on textile has preferable wash stability. Obviously, both wear and washing tests demonstrate that metal on textile printed by PDMS-assisted catalytic printing has excellent wear-resistance capability, which is derived from the ultrastrong adhesion capability between the metal and substrate.

CONCLUSIONS

In conclusion, PDMS-assisted catalytic printing is a new and simple strategy for fabricating flexible and foldable metal conductors on rough and porous paper or textile substrates. The key innovation of this strategy is the use of flexible and elastic PDMS as a matrix for AgNP catalysts so that the subsequent ELD can be carried out in situ to grow the highly precise, highly adhesive, and highly conductive metal conductors on the preprinted ink pattern. PDMS-assisted catalytic printing is a versatile strategy in the following aspects. First, the ink can be prepared by simply mixing the PDMS prepolymer, curing agent, and AgNPs without adding any solvents and additives, so the ink is nontoxic and environmentally friendly. Second, the ink can be directly screenprinted on rough and porous substrates (paper and textile) by adjusting the ratio of AgNPs to PDMS prepolymer, and highprecise patterns can be formed on substrates that are not pretreated. Third, PDMS-Ag ink as a viscoelastic fluid can coat microfibers of substrates, and cured ink can make the ELD metal embed into the PDMS matrix, so the PDMS-Ag composite can strongly bridge the ELD metal and substrate, resulting in a highly flexible Cu pattern on nylon (can be folded for at least 10,000 cycles and resist wear for at least 48,000 cycles). Fourth, the thickness and sheet resistance of metal can be controlled by tuning the ELD deposition time with low resistance and thus low energy loss in flexible and wearable electronics, for example, for a metal thickness of 81 μ m and the resistivity of about 2.36 \times 10⁻⁸ Ω m. Finally, the entire process consists of one printing process and two solution processes and operates at low temperatures; therefore, it is compatible with large-scale fabrication and roll-to-roll fabrication. Thus, PDMS-assisted catalytic printing shows remarkable application potentials for paper and textile electronics.

ASSOCIATED CONTENT

Solution Supporting Information

The Supporting Information is available free of charge at https://pubs.acs.org/doi/10.1021/acsami.1c18065.

Optical images, SEM images, and FT-IR spectra of PDMS-Ag ink without and with modifications of APTES; digital photographs of PDMS-Ag ink_{1.00} printed on the filter and sequent ELD Cu pattern; EDS mapping of the PDMS-Ag ink on filter paper; photographs and optical images of printed PDMS-Ag ink patterns with different mass ratios of AgNPs to PDMS; optical images of patterns on filter paper with printed inks stored after different months; XPS spectra of Ni/PDMS-Ag printed on filter paper; SEM cross-section view of Ni/PDMS-Ag on filter paper; adhesion cross-cut test of the Cu layer on the filter paper; oxidation-resistant properties of the printed Cu layer; roughness of substrates and the corresponding ink and Cu layer on substrates; optical images of the printed circuit with LEDs; and wash stability of the printed Cu layer on textile (PDF)

AUTHOR INFORMATION

Corresponding Authors

Hong Yu — State Key Laboratory of Solidification Processing, Center of Advanced Lubrication and Seal Materials, School of Materials Science and Engineering, Northwestern Polytechnical University, Xi'an, Shanxi 710072, China; orcid.org/0000-0002-1253-3475; Email: yh@nwpu.edu.cn

Qian Ye — State Key Laboratory of Solidification Processing, Center of Advanced Lubrication and Seal Materials, School of Materials Science and Engineering, Northwestern Polytechnical University, Xi'an, Shanxi 710072, China; orcid.org/0000-0003-2365-6304; Email: yeqian213@nwpu.edu.cn

Authors

Ruisheng Guo — State Key Laboratory of Solidification Processing, Center of Advanced Lubrication and Seal Materials, School of Materials Science and Engineering, Northwestern Polytechnical University, Xi'an, Shanxi 710072, China; State Key Laboratory of Solid Lubrication, Lanzhou Institute of Chemical Physics, Chinese Academy of Sciences, Lanzhou 730000, China; orcid.org/0000-0002-3131-2598

Haodong Li — State Key Laboratory of Solidification Processing, Center of Advanced Lubrication and Seal Materials, School of Materials Science and Engineering, Northwestern Polytechnical University, Xi'an, Shanxi 710072, China

Haoran Wang – State Key Laboratory of Solidification Processing, Center of Advanced Lubrication and Seal Materials, School of Materials Science and Engineering, Northwestern Polytechnical University, Xi'an, Shanxi 710072, China

Xiangyuan Zhao — State Key Laboratory of Solidification Processing, Center of Advanced Lubrication and Seal Materials, School of Materials Science and Engineering, Northwestern Polytechnical University, Xi'an, Shanxi 710072, China

Complete contact information is available at: https://pubs.acs.org/10.1021/acsami.1c18065

Author Contributions

R. G and H. L contributed equally. The manuscript was written through contributions of all authors. All authors have given approval to the final version of the manuscript.

Notes

The authors declare no competing financial interest.

ACKNOWLEDGMENTS

This work was financially supported by the National Natural Science Foundation of China (No. 51802265), the Natural Science Foundation of Shaanxi Province (2020JM-134), the Fundamental Research Funds for the Central Universities, and the Open Project of Key Laboratory of Solid Lubrication (LSL-1915). The authors would like to thank the Analytical and Testing Center of Northwestern Polytechnical University for analyzing the structures and performances of the asprepared materials.

ABBREVIATIONS

AgNPs, Ag nanoparticles
PDMS, polydimethylsiloxane
PDMS-Ag, composite of the PDMS prepolymer, curing
agent, and AgNPs
ELD, electroless deposition
PET, polyethylene terephthalate
PI, polyimide.

REFERENCES

- (1) Lee, H. M.; Choi, S. Y.; Jung, A.; Ko, S. H. Highly Conductive Aluminum Textile and Paper for Flexible and Wearable Electronics. *Angew. Chem. Int. Ed.* **2013**, *125*, 7872–7877.
- (2) Sevilla, G. A. T.; Inayat, S. B.; Rojas, J. P.; Hussain, A. M.; Hussain, M. M. Flexible and Semi-Transparent Thermoelectric Energy Harvesters from Low Cost Bulk Silicon (100). *Small* **2013**, *9*, 3916–3921.
- (3) Wang, H.; Ma, X.; Hao, Y. Electronic Devices for Human-Machine Interfaces. *Adv. Mater. Interfaces* **2017**, *4*, No. 1600709.
- (4) Zhang, Y. Z.; Wang, Y.; Cheng, T.; Yao, L. Q.; Li, X.; Lai, W. Y.; Huang, W. Printed Supercapacitors: Materials, Printing and Applications. *Chem. Soc. Rev.* **2019**, 48, 3229–3264.
- (5) Wu, W. Inorganic Nanomaterials for Printed Electronics: A Review. *Nanoscale* **2017**, *9*, 7342–7372.
- (6) Quinsaat, J. E. Q.; Burda, I.; Krämer, R.; Häfliger, D.; Nüesch, F. A.; Dascalu, M.; Opris, D. M. Conductive Silicone Elastomers Electrodes Processable by Screen Printing. Sci. Rep. 2019, 9, 13331.
- (7) Huang, Q.; Zhu, Y. Printing Conductive Nanomaterials for Flexible and Stretchable Electronics: A Review of Materials, Processes, and Applications. *Adv. Mater. Technol.* **2019**, *4*, No. 1800546.
- (8) Liu, Y.; Zhang, B.; Xu, Q.; Hou, Y.; Seyedin, S.; Qin, S.; Wallace, G. G.; Beirne, S.; Razal, J. M.; Chen, J. Development of Graphene Oxide/Polyaniline Inks for High Performance Flexible Microsupercapacitors Via Extrusion Printing. *Adv. Funct. Mater.* **2018**, 28, No. 1706592.

- (9) Zhang, C.; McKeon, L.; Kremer, M. P.; Park, S.-H.; Ronan, O.; Seral-Ascaso, A.; Barwich, S.; Coileáin, C. Ó.; McEvoy, N.; Nerl, H. C.; Anasori, B.; Coleman, J. N.; Gogotsi, Y.; Nicolosi, V. Additive-Free Mxene Inks and Direct Printing of Micro-Supercapacitors. *Nat. Commun.* **2019**, *10*, 1795.
- (10) Schmidt, G. C.; Panicker, P. M.; Qiu, X.; Benjamin, A. J.; Quintana Soler, R. A.; Wils, I.; Hübler, A. C. Paper-Embedded Roll-to-Roll Mass Printed Piezoelectric Transducers. *Adv. Mater.* **2021**, *33*, No. 2006437.
- (11) Zhou, Z.; Zhang, H.; Liu, J.; Huang, W. Flexible Electronics from Intrinsically Soft Materials. *Giant* **2021**, *6*, No. 100051.
- (12) Machiels, J.; Verma, A.; Appeltans, R.; Buntinx, M.; Ferraris, E.; Deferme, W. Printed Electronics (PE) as an Enabling Technology to Realize Flexible Mass Customized Smart Applications. *Procedia CIRP* **2021**, *96*, 115–120.
- (13) Siegel, A. C.; Phillips, S. T.; Dickey, M. D.; Lu, N.; Suo, Z.; Whitesides, G. M. Foldable Printed Circuit Boards on Paper Substrates. *Adv. Funct. Mater.* **2010**, 20, 28–35.
- (14) Eshkeiti, A.; Reddy, A. S.; Emamian, S.; Narakathu, B. B.; Joyce, M.; Joyce, M.; Fleming, P. D.; Bazuin, B. J.; Atashbar, M. Z. Screen Printing of Multilayered Hybrid Printed Circuit Boards on Different Substrates. *IEEE Trans. Compon. Packaging Manuf. Technol.* **2015**, *5*, 415–421.
- (15) Lu, Q.; Liu, L.; Yang, S.; Liu, J.; Tian, Q.; Yao, W.; Xue, Q.; Li, M.; Wu, W. Facile Synthesis of Amorphous FeOOH/MnO₂ Composites as Screen-Printed Electrode Materials for All-Printed Solid-State Flexible Supercapacitors. *J. Power Sources* **2017**, 361, 31–38
- (16) Stempien, Z.; Rybicki, E.; Rybicki, T.; Lesnikowski, J. Inkjet-Printing Deposition of Silver Electro-Conductive Layers on Textile Substrates at Low Sintering Temperature by Using an Aqueous Silver Ions-Containing Ink for Textronic Applications. *Sens. Actuators, B* **2016**, 224, 714–725.
- (17) Yao, B.; Zhang, J.; Kou, T.; Song, Y.; Liu, T.; Li, Y. Paper-Based Electrodes for Flexible Energy Storage Devices. *Adv. Sci.* **2017**, *4*, No. 1700107.
- (18) Liu, S.; Ma, K.; Yang, B.; Li, H.; Tao, X. Textile Electronics for VR/AR Applications. *Adv. Funct. Mater.* **2021**, *31*, No. 2007254.
- (19) Wang, Y.; Yan, C.; Cheng, S. Y.; Xu, Z. Q.; Sun, X.; Xu, Y. H.; Chen, J. J.; Jiang, Z.; Liang, K.; Feng, Z. S. Flexible RFID Tag Metal Antenna on Paper-Based Substrate by Inkjet Printing Technology. *Adv. Funct. Mater.* **2019**, 29, No. 1902579.
- (20) Kattumenu, R.; Rebros, M.; Joyce, M.; Hrehorova, E.; Fleming, P. D. Evaluation of Flexographically Printed Conductive Traces on Paper Substrates for RFID Applications. *TAGA J. Graph. Technol.* **2011**, *5*, 19–41.
- (21) Tai, H.; Duan, Z.; Wang, Y.; Wang, S.; Jiang, Y. Paper Based Sensors for Gas, Humidity, and Strain Detections: A Review. ACS Appl. Mater. Interfaces 2020, 12, 31037–31053.
- (22) Maddipatla, D.; Janabi, F.; Narakathu, B. B.; Ali, S.; Turkani, V. S.; Bazuin, B. J.; Fleming, P. D.; Atashbar, M. Z. Development of a Novel Wrinkle-Structure Based SERS Substrate for Drug Detection Applications. Sens. Bio-Sens. Res. 2019, 24, No. 100281.
- (23) Turkani, V. S.; Narakathu, B. B.; Maddipatla, D.; Altay, B. N.; Fleming, P. D.; Bazuin, B. J.; Atashbar, M. Z. Nickel Based Printed Resistance Temperature Detector on Flexible Polyimide Substrate. *IEEE Sensors* **2018**, 2018, 1–4.
- (24) Reddy, A.; Narakathu, B.; Atashbar, M.; Rebros, M.; Rebrosova, E.; Bazuin, B.; Joyce, M.; Fleming, P.; Pekarovicova, A. Printed Capacitive Based Humidity Sensors on Flexible Substrates. *Sensor Lett.* **2011**, *9*, 869–871.
- (25) Wang, Z.; Tammela, P.; Strømme, M.; Nyholm, L. Cellulose-Based Supercapacitors: Material and Performance Considerations. *Adv. Energy Mater.* **2017**, *7*, No. 1700130.
- (26) Liang, J.; Jiang, C.; Wu, W. Toward Fiber-, Paper-, and Foam-Based Flexible Solid-State Supercapacitors: Electrode Materials and Device Designs. *Nanoscale* **2019**, *11*, 7041–7061.

- (27) Dubal, D. P.; Chodankar, N. R.; Kim, D. H.; Gomez-Romero, P. Towards Flexible Solid-State Supercapacitors for Smart and Wearable Electronics. *Chem. Soc. Rev.* **2018**, *47*, 2065–2129.
- (28) Lee, S. S.; Choi, K. H.; Kim, S. H.; Lee, S. Y. Wearable Supercapacitors Printed on Garments. *Adv. Funct. Mater.* **2018**, 28, No. 1705571.
- (29) Zhang, Y.; Zhang, L.; Cui, K.; Ge, S.; Cheng, X.; Yan, M.; Yu, J.; Liu, H. Flexible Electronics Based on Micro/Nanostructured Paper. *Adv. Mater.* **2018**, *30*, No. 1801588.
- (30) Guo, R.; Chen, J.; Yang, B.; Liu, L.; Su, L.; Shen, B.; Yan, X. In-Plane Micro-Supercapacitors for an Integrated Device on One Piece of Paper. *Adv. Funct. Mater.* **2017**, 27, No. 1702394.
- (31) Guo, R.; Yu, Y.; Xie, Z.; Liu, X.; Zhou, X.; Gao, Y.; Liu, Z.; Zhou, F.; Yang, Y.; Zheng, Z. Matrix-Assisted Catalytic Printing for the Fabrication of Multiscale, Flexible, Foldable, and Stretchable Metal Conductors. *Adv. Mater.* **2013**, *25*, 3343–3350.
- (32) Yu, Y.; Zeng, J. F.; Chen, C. J.; Xie, Z.; Guo, R. S.; Liu, Z. L.; Zhou, X. C.; Yang, Y.; Zheng, Z. J. Three-Dimensional Compressible and Stretchable Conductive Composites. *Adv. Mater.* **2014**, *26*, 810–815
- (33) Liang, S.; Li, Y.; Yang, J.; Zhang, J.; He, C.; Liu, Y.; Zhou, X. 3D Stretchable, Compressible, and Highly Conductive Metal-Coated Polydimethylsiloxane Sponges. *Adv. Mater. Technol.* **2016**, *1*, No. 1600117.
- (34) Wang, D.; Zhang, Y.; Lu, X.; Ma, Z.; Xie, C.; Zheng, Z. Chemical Formation of Soft Metal Electrodes for Flexible and Wearable Electronics. *Chem. Soc. Rev.* **2018**, *47*, 4611–4641.
- (35) Raut, N.; al-Shamery, K. Inkjet Printing Metals on Flexible Materials for Plastic and Paper Electronics. *J. Mater. Chem. C* **2018**, *6*, 1618–1641.
- (36) Xie, J. Q.; Ji, Y. Q.; Kang, J. H.; Sheng, J. L.; Mao, D. S.; Fu, X. Z.; Sun, R.; Wong, C. P. In Situ Growth of Cu(OH)₂@FeOOH Nanotube Arrays on Catalytically Deposited Cu Current Collector Patterns for High-Performance Flexible In-Plane Micro-Sized Energy Storage Devices. *Energy Environ. Sci.* **2019**, *12*, 194–205.
- (37) Shahariar, H.; Jur, J. S. Correlation of Printing Faults with the RF Characteristics of Coplanar Waveguides (CPWs) Printed on Nonwoven Textiles. *Sens. Actuators, A* **2018**, *273*, 240–248.
- (38) Zhao, H.; Hou, L.; Wu, J. X.; Lu, Y. X. Fabrication of Dual-Side Metal Patterns onto Textile Substrates for Wearable Electronics by Combining Wax-Dot Printing with Electroless Plating. *J. Mater. Chem.* C **2016**, *4*, 7156–7164.
- (39) Lim, S.; Joyce, M.; Fleming, P. D.; Aijazi, A. T.; Atashbar, M. Inkjet Printing and Sintering of Nano-Copper Ink. *J. Imaging Sci. Technol.* **2013**, *57*, 50506-1.
- (40) Lim, S.; Fleming, P. D.; Joyce, M.; Lee, M. A Study of the Jetting Evolution of Nanocopper Ink and Nanosilver Ink with Inkjet. *J. Imaging Sci. Technol.* **2013**, *57*, 20506-1.
- (41) Shahariar, H.; Kim, I.; Soewardiman, H.; Jur, J. S. Inkjet Printing of Reactive Silver Ink on Textiles. *ACS Appl. Mater. Interfaces* **2019**, *11*, 6208–6216.
- (42) Choi, K.-H.; Yoo, J.; Lee, C. K.; Lee, S. Y. All-Inkjet-Printed, Solid-State Flexible Supercapacitors on Paper. *Energy Environ. Sci.* **2016**, *9*, 2812–2821.
- (43) Lessing, J.; Glavan, A. C.; Walker, S. B.; Keplinger, C.; Lewis, J. A.; Whitesides, G. M. Inkjet Printing of Conductive Inks with High Lateral Resolution on Omniphobic "RF Paper" for Paper-Based Electronics and MEMS. *Adv. Mater.* **2014**, *26*, 4677–4682.
- (44) Wolf, M. P.; Salieb-Beugelaar, G. B.; Hunziker, P. PDMS with Designer Functionalities—Properties, Modifications Strategies, and Applications. *Prog. Polym. Sci.* **2018**, *83*, 97–134.
- (45) Yuan, W.; Wu, X.; Gu, W.; Lin, J.; Cui, Z. Printed Stretchable Circuit on Soft Elastic Substrate for Wearable Application. *J. Semicond.* **2018**, 39, No. 015002.
- (46) Lin, Y.; Yuan, W.; Ding, C.; Chen, S.; Su, W.; Hu, H.; Cui, Z.; Li, F. Facile and Efficient Patterning Method for Silver Nanowires and Its Application to Stretchable Electroluminescent Displays. *ACS Appl. Mater. Interfaces* **2020**, *12*, 24074–24085.

- (47) Larmagnac, A.; Eggenberger, S.; Janossy, H.; Vörös, J. Stretchable Electronics Based on Ag-PDMS Composites. *Sci. Rep.* **2015**, *4*, 7254.
- (48) Soe, H. M.; Abd Manaf, A.; Matsuda, A.; Jaafar, M. Performance of a Silver Nanoparticles-Based Polydimethylsiloxane Composite Strain Sensor Produced Using Different Fabrication Methods. Sens. Actuators, A 2021, 329, No. 112793.
- (49) Spieser, H.; Jardin, A.; Deganello, D.; Gethin, D.; Bras, J.; Denneulin, A. Rheology of Cellulose Nanofibrils and Silver Nanowires for the Development of Screen-Printed Antibacterial Surfaces. *J. Mater. Sci.* **2021**, *56*, 12524–12538.
- (50) Wang, Y.; Wang, Y.; Chen, J. J.; Guo, H.; Liang, K.; Marcus, K.; Peng, Q. L.; Zhang, J.; Feng, Z. S. A Facile Process Combined with Inkjet Printing, Surface Modification and Electroless Deposition to Fabricate Adhesion-Enhanced Copper Patterns on Flexible Polymer Substrates for Functional Flexible Electronics. *Electrochim. Acta* **2016**, 218, 24–31.
- (51) Gian, P.; Shan, X.; Liang, Y.; Lok, B.; Lu, C.; Ooi, B. L. High Aspect Pattern Formation by Integration of Micro Inkjetting and Electroless Plating. In 2008 Symposium on Design, Test, Integration and Packaging of MEMS/MOEMS, 2008, pp. 162–167.
- (52) Jiang, J.; Bao, B.; Li, M.; Sun, J.; Zhang, C.; Li, Y.; Li, F.; Yao, X.; Song, Y. Fabrication of Transparent Multilayer Circuits by Inkjet Printing. *Adv. Mater.* **2016**, 28, 1420–1426.
- (53) Šun, J.; Guo, Y.; Cui, B.; Chu, F.; Li, H.; Li, Y.; He, M.; Ding, D.; Liu, R.; Li, L.; Song, Y. Inkjet Printing Bendable Circuits Based on An Oil-Water Interface Reaction. *Appl. Surf. Sci.* **2018**, *445*, 391–397.
- (54) Lee, J. N.; Park, C.; Whitesides, G. M. Solvent Compatibility of Poly(Dimethylsiloxane)-Based Microfluidic Devices. *Anal. Chem.* **2003**, *75*, 6544–6554.
- (55) Robinson, J.; Tarletgton, E.; Nijmeijer, A. Evidence for Swelling-Induced Pore Structure in Dense PDMS Nanofiltration Membranes. *Filtration* **2004**, *4*, 50–56.
- (56) Dogome, K.; Enomae, T.; Isogai, A. Method for Controlling Surface Energies of Paper Substrates to Create Paper-Based Printed Electronics. *Chem. Eng. Process.* **2013**, *68*, 21–25.
- (57) Huebner, G. Comparing Inkjet with Other Printing Processes and Mainly Screen Printing. In *Handbook of Industrial Inkjet Printing:* A Full System Approach; Wiley, 2017, pp. 7–22.
- (58) Ma, T.; Yang, R.; Zheng, Z.; Song, Y. Rheology of Fumed Silica/Polydimethylsiloxane Suspensions. *J. Rheol.* **2017**, *61*, 205–215.
- (59) Hengne, A. M.; Samal, A. K.; Enakonda, L. R.; Harb, M.; Gevers, L. E.; Anjum, D. H.; Hedhili, M. N.; Saih, Y.; Huang, K. W.; Basset, J. M. Ni–Sn-Supported ZrO₂ Catalysts Modified by Indium for Selective CO₂ Hydrogenation to Methanol. *ACS Omega* **2018**, *3*, 3688–3701.
- (60) Niu, X.; Peng, S.; Liu, L.; Wen, W.; Sheng, P. Characterizing and Patterning of PDMS-Based Conducting Composites. *Adv. Mater.* **2007**, *19*, 2682–2686.
- (61) Kim, J. Y.; Jang, K. S. Facile Fabrication of Stretchable Electrodes by Sedimentation of Ag Nanoparticles in PDMS Matrix. *J. Nanomater.* **2018**, 2018, No. 4580921.
- (62) Kausar, A. Polydimethylsiloxane-Based Nanocomposite: Present Research Scenario and Emergent Future Trends. *Polym. Plast. Technol. Mater.* **2020**, *59*, 1148–1166.